Jiří Maryška; Otto Severýn; Martin Vohralík
Mixed-hybrid model of the fracture flow

In: Jaromír Kuben and Jaromír Vosmanský (eds.): Equadiff 10, Czechoslovak International Conference on Differential Equations and Their Applications, Prague, August 27-31, 2001, [Part 2] Papers. Masaryk University, Brno, 2002. CD-ROM; a limited number of printed issues has been issued. pp. 297--321.

Persistent URL: http://dml.cz/dmlcz/700362

Equadiff 10, August 27–31, 2001
Prague, Czech Republic

Equadiff 10 CD ROM
Papers, pp. 297–321

Mixed-hybrid Model of the Fracture Flow

Jiří Maryška[1], Otto Severýn[2] and Martin Vohralík[3]

[1] Department of Modelling of Processes,
Faculty of Mechatronics and Interdisciplinary Engineering Studies,
Technical University of Liberec, Hálkova 6, 461 17 Liberec 1, Czech Republic
Email: jiri.maryska@vslib.cz
[2] Department of Modelling of Processes,
Faculty of Mechatronics and Interdisciplinary Engineering Studies,
Technical University of Liberec, Hálkova 6, 461 17 Liberec 1, Czech Republic
Email: otto.severyn@vslib.cz
[3] Department of Mathematics,
Faculty of Nuclear Sciences and Physical Engineering,
Czech Technical University in Prague, Trojanova 13, 120 00 Prague 2, Czech Republic
Email: vohralik@km1.fjfi.cvut.cz

Abstract. A stochastic discrete fracture network model of Darcy's underground water flow in disrupted rock massifs is introduced. Lowest order Raviart–Thomas mixed-hybrid FEM discretization is chosen, and it is properly imbedded in both the framework of mixed and mixed-hybrid FEM for the special conditions of the flow through connected system of 2-D polygons in 3-D. Model problems are tested and generation and triangulation of fracture networks for real situations is described.

MSC 2000. 76M10, 65C20, 65N50, 65N15, 35J25

Keywords. Fracture flow, stochastic discrete fracture network model, mixed and mixed-hybrid finite element method

1 Introduction

We consider a steady saturated Darcy's law governed flow of an incompressible fluid through a system of 2-D polygons placed in the 3-D space and connected under certain conditions into one network. This may simulate underground water flow through natural geological disruptions of a rock massif, fractures, e.g. for the purposes of finding suitable nuclear waste repositories. Note that intersection of

three or more triangles through one edge in the discretization is possible owing to the special geometrical situation, see Fig 11. We use the lowest order Raviart-Thomas mixed-hybrid finite element approximation, and we study its existence and uniqueness, existence and uniqueness of appropriate weak solutions, and the approximation error in the framework of the mixed FEM and the mixed-hybrid FEM, see [10], [8] respectively. For technical details of the following, see [14].

The outline of the contribution is as follows: in Section 2, we state the mathematical-physical formulation, in Section 3, we give appropriate function spaces, in Section 4, we state the weak primal formulation and verify its existence and uniqueness, which we will need in Sections 5 and 6 in order to prove the existence and uniqueness of weak and discrete solutions for the mixed/mixed hybrid finite element methods. The theoretical estimates are confirmed by the carried out numerical examples, see Section 7. Description of stochastic discrete fracture networks generation and discretization for simulation of real situations is given in Section 8.

2 Mathematical-physical Formulation

We suppose that we have

$$\mathcal{S} \;=\; \left\{ \bigcup_{\ell \in L} \overline{\alpha_\ell} \setminus \partial \mathcal{S} \right\}, \tag{1}$$

where α_ℓ is an opened 2-D polygon placed in a 3-D Euclidean space; we call $\overline{\alpha_\ell}$ as a fracture. We denote as L the index set of fractures, $|L|$ is the number (finite) of considered fractures. We suppose that all closures of these polygons are connected into one "fracture network", the connection is possible only through an edge, not a point. Moreover, we require that if $\overline{\alpha_i} \bigcap \overline{\alpha_j} \neq \emptyset$ then $\overline{\alpha_i} \bigcap \overline{\alpha_j} \subset \partial\alpha_i \bigcap \partial\alpha_j$, i.e. the connection is possible only through fracture boundaries (we state this requirement in order to be able to define correct function spaces). The situation is schematically viewed in Figure 4.

Let us have a 2-D orthogonal coordinate system in each polygon α_ℓ. We are looking for the fracture flow velocity $\mathbf{u}$ (2-D vector in each α_ℓ), which is the solution of the following problem

$$\mathbf{u} = -\mathbf{K}\Big(\nabla p + \nabla z\Big) \quad \text{in} \quad \mathcal{S}\,, \tag{2}$$

$$\nabla \cdot \mathbf{u} = q \quad \text{in} \quad \mathcal{S}\,, \tag{3}$$

$$p = p_D \quad \text{in} \quad \Lambda_D, \qquad \mathbf{u}\cdot\mathbf{n} - \sigma(p - p_D) = u_N \quad \text{in} \quad \Lambda_N\,, \tag{4}$$

where all variables are expressed in local coordinates of appropriate α_ℓ and also the differentiation is always expressed towards these local coordinates. The equation (2) is Darcy's law, (3) is the mass balance equation and (4) is the expression of

appropriate boundary conditions. The variable p denotes the modified fluid pressure p ($p = \frac{\mathrm{p}}{\varrho g}$), g is the gravitational acceleration constant, ϱ is the fluid density, q represents stationary sources/sinks density and z is the elevation, positive upward taken vertical 3-D coordinate expressed in appropriate local coordinates.

We require the second rank tensor $\mathbf{K}$ to be symmetric and uniformly positive definite on each α_ℓ, i.e. $\sum_{i,j=1}^{2} K_{ij}(\mathbf{x})\eta_i\eta_j \geq \beta \sum_{i=1}^{2} \eta_i^2$, $\beta > 0$ for any $(\eta_1, \eta_2) \in \mathbb{R}^2$ and almost all $\mathbf{x} \in \overline{\alpha_\ell} \setminus \partial\mathcal{S}$, for all $\ell \in L$, and pose also the requirement $\Lambda_D \cap \Lambda_N = \emptyset$, $\overline{\Lambda}_D \cup \overline{\Lambda}_N = \partial\mathcal{S}$, $\Lambda_D \neq \emptyset$.

3 Function Spaces

We start from $L^2(\alpha_\ell)$, $\|u\|_{0,\alpha_\ell} = (\int_{\alpha_\ell} u^2 \, dS)^{\frac{1}{2}}$ and $\mathbf{L}^2(\alpha_\ell) = L^2(\alpha_\ell) \times L^2(\alpha_\ell)$ in order to introduce

$$L^2(\mathcal{S}) \equiv \prod_{\ell \in L} L^2(\alpha_\ell)\,, \quad \mathbf{L}^2(\mathcal{S}) \equiv L^2(\mathcal{S}) \times L^2(\mathcal{S})\,. \tag{5}$$

We begin with classical Sobolev space $H^1(\alpha_\ell)$ of scalar functions with square integrable weak derivatives, $H^1(\alpha_\ell) = \{\varphi \in L^2(\alpha_\ell);\ \nabla\varphi \in \mathbf{L}^2(\alpha_\ell)\}$, $\|\varphi\|_{1,\alpha_\ell} = (\int_{\alpha_\ell} [\varphi^2 + \nabla\varphi \cdot \nabla\varphi] \, dS)^{\frac{1}{2}}$, so as to introduce

$$\begin{aligned} &H^1(\mathcal{S}) \equiv \{v \in L^2(\mathcal{S})\,;\, v|_{\alpha_\ell} \in H^1(\alpha_\ell) \quad \forall \ell \in L\,, \\ &(v|_{\alpha_i})|_f = (v|_{\alpha_j})|_f \quad \forall\, f = \overline{\alpha_i} \bigcap \overline{\alpha_j}\,,\ i,j \in L\,\}\,. \end{aligned} \tag{6}$$

We then have the spaces $H^{\frac{1}{2}}(\partial\mathcal{S})$ and $H^{-\frac{1}{2}}(\partial\mathcal{S})$ and the surjective continuous trace operator $\gamma : H^1(\mathcal{S}) \to H^{\frac{1}{2}}(\partial\mathcal{S})$ as in the standard "planar" case. We further can define $H^1_D(\mathcal{S}) = \{\varphi \in H^1(\mathcal{S})\ ;\ \gamma\varphi = 0 \ \text{ on } \ \Lambda_D\}$, $H^{\frac{1}{2}}(\Lambda_N) = \{\mu : \Lambda_N \to \mathbb{R};\ \exists\, \varphi \in H^1_D(\mathcal{S}),\ \mu = \gamma\varphi\}$, $H^{-\frac{1}{2}}(\Lambda_N) = \{\psi \in H^{-\frac{1}{2}}(\partial\mathcal{S}); \langle\psi, \varphi\rangle_{\partial\mathcal{S}} = 0\ \forall\varphi \in H^1_N(\mathcal{S})\}$ and, for $p_d \in H^{\frac{1}{2}}(\Lambda_D)$, $H^1_{D,*}(\mathcal{S}) = \{\varphi \in H^1(\mathcal{S})\ ;\ \gamma\varphi = p_D \ \text{ on } \ \Lambda_D\}$.

We denote as $\mathbf{H}(div, \alpha_\ell)$ the Hilbert space of vector functions with square integrable weak divergences, $\mathbf{H}(div, \alpha_\ell) = \{\mathbf{v} \in \mathbf{L}^2(\alpha_\ell); \nabla\cdot\mathbf{v} \in L^2(\alpha_\ell)\}$, $\|\mathbf{v}\|_{\mathbf{H}(div,\alpha_\ell)} = (\|\mathbf{v}\|^2_{0,\alpha_\ell} + \|\nabla\cdot\mathbf{v}\|^2_{0,\alpha_\ell})^{\frac{1}{2}}$. We can define now

$$\begin{aligned} &\mathbf{H}(div, \mathcal{S}) \equiv \{v \in \mathbf{L}^2(\mathcal{S})\,;\, \mathbf{v}|_{\alpha_\ell} \in \mathbf{H}(div, \alpha_\ell) \quad \forall \ell \in L\,, \\ &\qquad \textstyle\sum_{i \in I_f} \langle \mathbf{v}|_{\alpha_i} \cdot \mathbf{n}_i, \varphi_i\rangle = 0 \\ &\forall f \text{ such that } |I_f| \geq 2\,,\ I_f = \{i \in L\,;\, f \subset \partial\alpha_i\}\,,\ \forall \varphi_i \in H^1_{\partial\alpha_i \setminus f}\,. \end{aligned} \tag{7}$$

We have the surjective continuous normal trace operator $\zeta : \mathbf{u} \in \mathbf{H}(div, \mathcal{S}) \to \mathbf{u}\cdot\mathbf{n} \in H^{-\frac{1}{2}}(\partial\mathcal{S})$ as in the standard "planar" case. We further define the space $\mathbf{H}_{0,N}(div, \mathcal{S}) = \{\mathbf{u} \in \mathbf{H}(div, \mathcal{S})\ ;\ \langle \mathbf{u}\cdot\mathbf{n}, \varphi\rangle_{\partial\mathcal{S}} = 0 \quad \forall\varphi \in H^1_D(\mathcal{S})\}$. The norms on the spaces defined by (5), (6), (7) are given as

$$\|\ \|^2_{\cdot,\mathcal{S}} = \sum_{\ell=1}^{|L|} \|\ \|^2_{\cdot,\alpha_\ell}\,. \tag{8}$$

Remark 1. Note that definitions (5), (6), (7) are essential. The system $\mathcal{S}$, however consisting of plane polygons, is not plane by oneself. Moreover, one edge can be common to three or more polygons α_ℓ creating the system $\mathcal{S}$. Hence the definition of the space $H^1(\mathcal{S})$ of scalar continuous functions and especially of $\mathbf{H}(div, \mathcal{S})$ of normal trace vector continuous functions, expressing the mass balance condition at each inner edge. Note also that these definitions coincide with the classical ones for at most two polygons intersecting through one edge, cf. [11, Theorem 1.3.]

We now turn to function spaces necessary for the mixed-hybrid formulation. Let us thus suppose a triangulation of the system $\mathcal{S}$; we require that the triangulation in each fracture incorporates the intersections with other fractures. We define an index set J_h to number the elements of the triangulation $\mathcal{T}_h$, $|J_h|$ denotes the number of elements. We define two sets of edges,

$$\Lambda_h = \cup_{e\in\mathcal{T}_h} \partial e \quad , \quad \Lambda_{h,D} = \cup_{e\in\mathcal{T}_h} \partial e \setminus \Lambda_D \,, \tag{9}$$

and on $\Lambda_{h,D}$, we set

$$H^{\frac{1}{2}}(\Lambda_{h,D}) = \{\mu :\, \Lambda_{h,D} \to \mathbb{R}\,;\; \exists \varphi \in H^1_D(\mathcal{S}),\; \mu^e = \gamma_h \varphi^e \quad \forall e \in \mathcal{T}_h \}\,, \tag{10}$$

where γ_h is the trace mapping of functions from $H^1_D(\mathcal{S})$ on the edges structure $\Lambda_{h,D}$. For the functions from $H^{\frac{1}{2}}(\Lambda_{h,D})$, we have the norm

$$|\mu|_{\frac{1}{2},\Lambda_{h,D}} = \inf_{\varphi\in H^1_D(\mathcal{S})} \{|\varphi|_{1,\mathcal{S}}\,;\, \mu^e = \gamma_h \varphi^e \quad \forall e \in \mathcal{T}_h\}\,.$$

Due to $\Lambda_D \neq \emptyset$, $|\cdot|_{\frac{1}{2},\Lambda_{h,D}}$ is a norm on $\Lambda_{h,D}$ equivalent with $\|\cdot\|_{\frac{1}{2},\Lambda_{h,D}}$. This definition will be suitable later in order to obtain the inf–sup condition.

The standard hybrid-divergence space $\mathbf{H}(div, \mathcal{T}_h)$ without any continuity requirements has the form

$$\mathbf{H}(div, \mathcal{T}_h) = \{\mathbf{v} \in \mathbf{L}^2(\mathcal{S})\,;\; \nabla\cdot\mathbf{v}^e \in L^2(e)\;\; \forall e \in \mathcal{T}_h\}\,, \tag{11}$$

with the norm $\|\mathbf{v}\|^2_{\mathbf{H}(div,\mathcal{T}_h)} = \sum_{\ell=1}^{|L|} \|\mathbf{v}\|^2_{0,\alpha_\ell} + \sum_{\ell=1}^{|J_h|} \|\nabla\cdot\mathbf{v}\|^2_{0,e_\ell}$.

4 Existence and Uniqueness of the Primal Formulation

Let us suppose that we have a $\tilde{p}$ such that $\tilde{p} \in H^1_{D,*}(\mathcal{S})$.

Definition 2. As a primal weak solution of the steady saturated fracture flow problem described by (2) - (4) on the system $\mathcal{S}$, we understand a function $p = p_0 + \tilde{p}$, $p_0 \in H^1_D(\mathcal{S})$, such that

$$\begin{aligned}(\mathbf{K}\nabla p_0, \nabla\varphi)_{0,\mathcal{S}} + \langle \sigma p_0, \varphi\rangle_{\Lambda_N} = (q,\varphi)_{0,\mathcal{S}} + \langle \sigma p_D - u_N, \varphi\rangle_{\Lambda_N} - \\ -(\mathbf{K}\nabla z, \nabla\varphi)_{0,\mathcal{S}} - (\mathbf{K}\nabla\tilde{p}, \nabla\varphi)_{0,\mathcal{S}} - \langle \sigma\tilde{p}, \varphi\rangle_{\Lambda_N} \qquad \forall \varphi \in H^1_D(\mathcal{S})\,.\end{aligned} \tag{12}$$

Our general requirements are $K_{ij} \in L^\infty(\mathcal{S})$, $q \in L_2(\mathcal{S})$, $p_D \in H^{\frac{1}{2}}(\Lambda_D \cup \Lambda_N)$, $u_N \in H^{-\frac{1}{2}}(\Lambda_N)$ and $\sigma \in L^\infty(\Lambda_N)$, $0 \le \sigma \le \sigma_M$.

Theorem 3. *The problem* (12) *has a unique solution.*

Proof. Considering standard techniques (triangle inequality, bound $|K_{ij}(\mathbf{x})| \leq K$, Schwarz's inequality, positive definiteness of the tensor $\mathbf{K}$ on each α_ℓ, estimates for Sobolev spaces $H^1(\alpha_\ell)$, $\Lambda_D \neq \emptyset$) and the definition of all norms like in (8), the only crucial point is the use of Hölder's inequality

$$(\textstyle\sum_{i=1}^n a_i^2)^{\frac{1}{2}}(\sum_{i=1}^n b_i^2)^{\frac{1}{2}} \geq \sum_{i=1}^n a_i b_i,\ \ a_i, b_i \in \mathbb{R}\,. \tag{13}$$

The term $\|z\|_{1,\mathcal{S}}$ is surely finite, since in each fracture, the 3-D z coordinate is expressed in its local coordinates as a linear function, and ∇z is thus a constant vector in each α_ℓ, $\ell \in L$. We have that the left hand side of (12) represents a bilinear continuous form on $H^1_D(\mathcal{S}) \times H^1_D(\mathcal{S})$, coercive on $H^1_D(\mathcal{S})$, and since the right hand side of (12) represents a linear continuous functional on $H^1_D(\mathcal{S})$, the assertion is assured by the Lax–Milgram lemma.

5 Mixed FEM and Subsequent Hybridization

Although the possibility to use the mixed finite element method is not apparent at the first sight because of the special geometrical situation treated, we will see that it is possible due to the special function spaces introduced in Section 3 and special approximation spaces introduced in this section, considering also the existence and uniqueness of the primal formulation. We take $\sigma = 0$, i.e. the problem (2) - (4) with only Neumann boundary conditions.

5.1 Weak Mixed Solution

The tensor of the fracture hydraulic conductivity $\mathbf{K}$ is positive definite on each α_ℓ, and therefore there exists, on each α_ℓ, a positive definite tensor $\mathbf{A} = \mathbf{K}^{-1}$ which characterizes the medium resistance. Let us now consider such $\tilde{\mathbf{u}}$ that $\tilde{\mathbf{u}} \cdot \mathbf{n} = u_N$ on Λ_N in appropriate sense.

Definition 4. As a weak mixed solution of the steady saturated fracture flow problem described by (2) – (4), we understand functions $\mathbf{u} = \mathbf{u}_0 + \tilde{\mathbf{u}}$, $\mathbf{u}_0 \in \mathbf{H}_{0,N}(div, \mathcal{S})$, and $p \in L^2(\mathcal{S})$ satisfying

$$\begin{aligned}(\mathbf{A}\mathbf{u}_0, \mathbf{v})_{0,\mathcal{S}} - (\nabla \cdot \mathbf{v}, p)_{0,\mathcal{S}} = -\langle \mathbf{v} \cdot \mathbf{n}, p_D \rangle_{\Lambda_D} + (\nabla \cdot \mathbf{v}, z)_{0,\mathcal{S}} - \\ -\langle \mathbf{v} \cdot \mathbf{n}, z \rangle_{\partial\mathcal{S}} - (\mathbf{A}\tilde{\mathbf{u}}, \mathbf{v})_{0,\mathcal{S}} \qquad \forall\, \mathbf{v} \in \mathbf{H}_{0,N}(div, \mathcal{S})\,,\end{aligned} \tag{14}$$

$$-(\nabla \cdot \mathbf{u}_0, \phi)_{0,\mathcal{S}} = -(q, \phi)_{0,\mathcal{S}} + (\nabla \cdot \tilde{\mathbf{u}}, \phi)_{0,\mathcal{S}} \qquad \forall \phi \in L^2(\mathcal{S})\,. \tag{15}$$

Our general requirements are $A_{ij} \in L^\infty(\mathcal{S})$, $q \in L_2(\mathcal{S})$, $p_D \in H^{\frac{1}{2}}(\Lambda_D)$ and $u_N \in H^{-\frac{1}{2}}(\Lambda_N)$.

Theorem 5. *The problem* (14), (15) *has a unique solution.*

Proof. Let us denote

$$a(\mathbf{u},\mathbf{v}) = (\mathbf{A}\mathbf{u},\mathbf{v})_{0,\mathcal{S}} = \sum_{\ell=1}^{|L|} \int_{\alpha_\ell} \mathbf{A}\mathbf{u}\cdot\mathbf{v}\; dS\,,$$

$$b(\mathbf{v},\phi) = (\nabla\cdot\mathbf{v},\phi)_{0,\mathcal{S}} = \sum_{\ell=1}^{|L|} \int_{\alpha_\ell} \nabla\cdot\mathbf{v}\;\phi\; dS\,,$$

$f(\mathbf{v})$ and $g(\phi)$ the functionals on the right hand sides of (14), (15) respectively, and $\mathbf{V} = \mathbf{H}_{0,N}(div,\mathcal{S})$, $\Phi = L^2(\mathcal{S})$, and $\mathbf{W} = \{\mathbf{v}\in\mathbf{V}\;;\; b(\mathbf{v},\phi) = 0 \quad \forall\phi\in\Phi\}$. It is easy then to show that the form $a(\cdot,\cdot)$ is a bilinear continuous form on $\mathbf{V}\times\mathbf{V}$, moreover coercive on $\mathbf{W}$, the form $b(\cdot,\cdot)$ is a bilinear continuous form on $\mathbf{V}\times\Phi$ satisfying the inf–sup (Babuška–Brezzi) condition

$$\inf_{\phi\in\Phi}\sup_{\mathbf{v}\in\mathbf{V}} \frac{b(\mathbf{v},\phi)}{\|\mathbf{v}\|_{\mathbf{H}(div,\mathcal{S})}\|\phi\|_{(0,\mathcal{S})}} \geq k_1 \tag{16}$$

with $k_1 > 0$. Further, the functional $f(\cdot)$ is a linear continuous functional on $\mathbf{V}$ and the functional $g(\cdot)$ is a linear continuous functional on Φ. The proofs are direct applications of standard techniques; essential is the existence and uniqueness of the primal solution and again Hölder's inequality (13), see [14] for details. Using [11, Theorem 10.1.] (originally Brezzi 1974), we have the assertion.

5.2 Mixed Finite Element Approximation

We define a 3-dimensional space $\mathbf{RT}^0(e)$ of vector functions linear on a given element e with the basis $\mathbf{v}_i^e$, $i\in\{1,2,3\}$, where

$$\mathbf{v}_1^e = k_1^e\begin{bmatrix} x-\alpha_{11}^e \\ y-\alpha_{12}^e\end{bmatrix},\quad \mathbf{v}_2^e = k_2^e\begin{bmatrix} x-\alpha_{21}^e \\ y-\alpha_{22}^e\end{bmatrix},\quad \mathbf{v}_3^e = k_3^e\begin{bmatrix} x-\alpha_{31}^e \\ y-\alpha_{32}^e\end{bmatrix}.$$

Concerning its dual basis, we state classically N_j^e, $j=1,2,3$, $N_j^e(\mathbf{u}_h) = \int_{f_j^e}\mathbf{u}_h\cdot\mathbf{n}_j^e\,dl$, where each functional N_j^e expresses the flux through one edge for $\mathbf{u}_h\in\mathbf{RT}^0(e)$; we have $N_j^e(\mathbf{v}_i^e) = \delta_{ij}$ after appropriate choice of $\alpha_{11}^e - \alpha_{32}^e$, $k_1^e - k_3^e$. The local interpolation operator is then given by

$$\pi_e(\mathbf{u}) = \sum_{i=1}^{3} N_i^e(\mathbf{u})\mathbf{v}_i^e \quad \forall\;\mathbf{u}\in(H^1(e))^2\,. \tag{17}$$

We start from the Raviart–Thomas space $\mathbf{RT}^0_{-1}(\mathcal{T}_h)$ of on each element linear vector functions without any continuity requirements,

$$\mathbf{RT}^0_{-1}(\mathcal{T}_h) \equiv \{\mathbf{v}\in\mathbf{L}^2(\mathcal{S})\;;\; \mathbf{v}|_e\in\mathbf{RT}^0(e)\quad\forall e\in\mathcal{T}_h\}\,,$$

to define the necessary "continuity assuring" space $\mathbf{RT}^0_0(\mathcal{T}_h)$ by

$$\mathbf{RT}^0_0(\mathcal{T}_h) \equiv \{\mathbf{v}\in\mathbf{RT}^0_{-1}(\mathcal{T}_h)\;;\; \textstyle\sum_{i\in I_f}\mathbf{v}|_{e_i}\cdot\mathbf{n}_{f,\partial e_i} = 0\;\forall f \text{ such that}$$
$$|I_f|\geq 2\,,\; I_f = \{i\in J_h\;;\; f\subset\partial e_i\} = \mathbf{RT}^0_{-1}(\mathcal{T}_h)\cap\mathbf{H}(div,\mathcal{S})\,.$$

We set furthermore

$$\mathbf{RT}^0_{0,N}(\mathcal{T}_h) \equiv \{\mathbf{v} \in \mathbf{RT}^0_0(\mathcal{T}_h)\,;\ \mathbf{v}\cdot\mathbf{n} = 0 \text{ in } \Lambda_N\} = \mathbf{RT}^0_{-1}(\mathcal{T}_h) \cap \mathbf{H}_{0,N}(div, \mathcal{S})$$

and

$$M^0_{-1}(\mathcal{T}_h) \ \equiv\ \{\phi \in L^2(\mathcal{S})\,;\, \phi|_e \in M^0(e) \quad \forall e \in \mathcal{T}_h\}\,,$$

where $M^0(e)$ is the space of scalar functions constant on a given element e. Looking for the basis, appropriate dual basis, and global interpolation operator for $\mathbf{RT}^0_0(\mathcal{T}_h)$, we have the following definitions and lemmas:

We set $\mathcal{N}_h = \{N_1, N_2, \ldots, N_{I_{\mathcal{N}_h}}\}$ as the dual basis of $\mathbf{RT}^0_0(\mathcal{T}_h)$, where for each border edge f, we have one functional N_f defined by $N_f(\mathbf{u}_h) = \int_f \mathbf{u}_h|_e \cdot \mathbf{n}_{\partial e}\, dl$, and for each inner edge f common to elements $e_1, e_2, \ldots, e_{I_f}$, we have $I_f - 1$ functionals given by

$$N_{f,j}(\mathbf{u}_h) = \frac{1}{I_f}\int_f \mathbf{u}_h|_{e_1}\cdot\mathbf{n}_{\partial e_1}\, dl - \frac{1}{I_f}\int_f \mathbf{u}_h|_{e_{j+1}}\cdot\mathbf{n}_{\partial e_{j+1}}\, dl \quad , \quad j = 1, \ldots, I_f - 1\,.$$

Lemma 6. *For all $\mathbf{u}_h \in \mathbf{RT}^0_0(\mathcal{T}_h)$, from $N_j(\mathbf{u}_h) = 0\ \forall\ j = 1, \ldots, I_{\mathcal{N}_h}$ follows that $\mathbf{u}_h = 0$.*

Proof. Let us suppose that $N_j(\mathbf{u}_h) = 0\ \forall\ j = 1, \ldots, I_{\mathcal{N}_h}$. From the definition of the functionals N_f on border edges, we have $\int_f \mathbf{u}_h|_e \cdot \mathbf{n}_{\partial e}\, dl = 0$ for all border edges f. Concerning the definition of the functionals $N_{f,j}$ on inner edges and the condition $N_{f,j}(\mathbf{u}_h) = 0$, we have $\int_f \mathbf{u}_h|_{e_1}\cdot\mathbf{n}_{\partial e_1}\, dl = \int_f \mathbf{u}_h|_{e_j}\cdot\mathbf{n}_{\partial e_j}\, dl$ for all $j = 2, \ldots, I_f$. Considering the equality $\sum_{i=1}^{I_f}\int_f \mathbf{u}_h|_{e_i}\cdot\mathbf{n}_{\partial e_i}\, dl = 0$ characterizing the continuity of the functions from $\mathbf{RT}^0_0(\mathcal{T}_h)$, we come to $\int_f \mathbf{u}_h|_e\cdot\mathbf{n}_{\partial e}\, dl = 0$ for all $f \in \Lambda_h$ and all e, $f \subset e$. Since $\mathbf{RT}^0_0(\mathcal{T}_h) \subset \mathbf{RT}^0_{-1}(\mathcal{T}_h)$ and all coefficients for the local interpolants on each $e \in \mathcal{T}_h$ are equal to zero, $\mathbf{u}_h = 0$ follows.

We set $\mathcal{V}_h = \{\mathbf{v}_1, \mathbf{v}_2, \ldots, \mathbf{v}_{I_{\mathcal{N}_h}}\}$, where for each border edge f, we have one base function $\mathbf{v}_f$ defined by $\mathbf{v}_f = \mathbf{v}^e_f$ with $\mathbf{v}^e_f$ being the local base function appropriate to the element e and its edge f, and for each inner edge f common to elements $e_1, e_2, \ldots, e_{I_f}$, we have $I_f - 1$ base functions given by

$$\mathbf{v}_{f,i} = \sum_{k=1,\ k\neq i+1}^{I_f} \mathbf{v}^{e_k}_f - (I_f - 1)\mathbf{v}^{e_{i+1}}_f \quad , \quad i = 1, \ldots, I_f - 1\,.$$

Lemma 7. *For the bases $\mathcal{N}_h$ and $\mathcal{V}_h$, $N_j(\mathbf{v}_i) = \delta_{ij}$, $i, j = 1, \ldots, I_{\mathcal{N}_h}$ holds.*

Proof. We have from the definition of base functions of $\mathbf{RT}^0(e)$ that $N_f(\mathbf{v}_f) = 1$ for all border edges f, and simply $N_f(\mathbf{v}) = 0$ for all $\mathbf{v} \in \mathcal{V}_h$, $\mathbf{v} \neq \mathbf{v}_f$. Concerning the inner edges, we easily come to $N_{f,j}(\mathbf{v}_g) = 0$ for all $j = 1, \ldots, I_f - 1$, f an inner edge, g border edge, and to $N_{f,j}(\mathbf{v}_{g,i}) = 0$ for all $j = 1, \ldots, I_f - 1$, $i = 1, \ldots, I_g - 1$, f an inner edge, g another inner edge. We have

$$N_{f,j}(\mathbf{v}_{f,i}) = \frac{1}{I_f}\int_f \mathbf{v}^{e_1}_f\cdot\mathbf{n}_{\partial e_1}\, dl - \frac{1}{I_f}\int_f \mathbf{v}^{e_{j+1}}_f\cdot\mathbf{n}_{\partial e_{j+1}}\, dl = \frac{1}{I_f} - \frac{1}{I_f} = 0$$

for $i \neq j$, and

$$N_{f,j}(\mathbf{v}_{f,i}) = \frac{1}{I_f}\int_f \mathbf{v}_f^{e_1}\cdot\mathbf{n}_{\partial e_1}\ dl - \frac{1}{I_f}\int_f -(I_f-1)\mathbf{v}_f^{e_{j+1}}\cdot\mathbf{n}_{\partial e_{j+1}}\ dl = \\ = \frac{1}{I_f} + \frac{1}{I_f}(I_f-1) = 1$$

for $i = j$, $i, j = 1, \ldots, I_f - 1$, f an inner edge. Thus the proof is completed.

We introduce first a space smoother than $\mathbf{H}(div, \mathcal{S})$, corresponding to the classical $(H^1(\mathcal{S}))^2$,

$$\begin{gathered}\mathbf{H}(grad, \mathcal{S}) = \{v \in \mathbf{L}^2(\mathcal{S})\,;\, \mathbf{v}|_{\alpha_\ell} \in (H^1(\alpha_\ell))^2 \quad \forall \ell \in L\,, \\ \textstyle\sum_{i\in I_f} \mathbf{v}|_{\alpha_i}\cdot\mathbf{n}_{f,\partial\alpha_i} = 0 \\ \forall f \text{ such that } |I_f| \geq 2\,,\ I_f = \{i \in L\,;\, f \subset \partial\alpha_i\}\,,\end{gathered} \tag{18}$$

in order to set the global interpolation operator

$$\pi_h(\mathbf{u}) = \sum_{i=1}^{I_{\mathcal{N}_h}} N_i(\mathbf{u})\mathbf{v}_i \quad \forall\ \mathbf{u} \in \mathbf{H}(grad, \mathcal{S})\,. \tag{19}$$

Lemma 8. *Concerning the local and global interpolation operators given by* (17), (19) *respectively, we have their equality on each element, i.e.*

$$\pi_h(\mathbf{u})|_e = \pi_e(\mathbf{u}|_e) \quad \forall\ e \in \mathcal{T}_h,\ \forall\ \mathbf{u} \in \mathbf{H}(grad, \mathcal{S})\,.$$

Proof. As the the base functions $\mathbf{v}_i$, $i = 1, \ldots, I_{\mathcal{N}_h}$ of $\mathbf{RT}_0^0(\mathcal{T}_h)$ are combined from the base functions $\mathbf{v}_j^e$ on each element, we only have to verify that the coefficients by $\mathbf{v}_j^e$ are the same. By border edges, the situation is apparent – the coefficients for both local and global interpolation operators are given by $\int_f \mathbf{u}|_e\cdot\mathbf{n}_{\partial e}\ dl$. For the inner edges, we have

$$\Big\{\sum_{i=1}^{I_f-1} N_{f,i}(\mathbf{u})\mathbf{v}_{f,i}\Big\}\Big|_{e_j} = \Big\{\sum_{i=1}^{I_f-1}\Big(\frac{1}{I_f}\int_f \mathbf{u}|_{e_1}\cdot\mathbf{n}_{\partial e_1}\ dl - \frac{1}{I_f}\int_f \mathbf{u}|_{e_{i+1}}\cdot\mathbf{n}_{\partial e_{i+1}}\ dl\Big)\cdot \\ \Big(\sum_{k=1,\ k\neq i+1}^{I_f} \mathbf{v}_f^{e_k} - (I_f-1)\mathbf{v}_f^{e_{i+1}}\Big)\Big\}\Big|_{e_j} = \sum_{i=1,\ i\neq j-1}^{I_f-1}\Big(\frac{1}{I_f}\int_f \mathbf{u}|_{e_1}\cdot\mathbf{n}_{\partial e_1}\ dl - \\ -\frac{1}{I_f}\int_f \mathbf{u}|_{e_{i+1}}\cdot\mathbf{n}_{\partial e_{i+1}}\ dl\Big)\cdot\mathbf{v}_f^{e_j} - (1-\delta_{j1})\Big(\frac{1}{I_f}\int_f \mathbf{u}|_{e_1}\cdot\mathbf{n}_{\partial e_1}\ dl - \\ -\frac{1}{I_f}\int_f \mathbf{u}|_{e_j}\cdot\mathbf{n}_{\partial e_j}\ dl\Big)\cdot(I_f-1)\mathbf{v}_f^{e_j}$$

using the definition of $N_{f,i}$ and $\mathbf{v}_{f,i}$ for an inner edge f, $i = 1, \ldots, I_f - 1$, $j = 1, \ldots, I_f$. Considering now only the coefficients by $\mathbf{v}_f^{e_j}$, we come to

$$\sum_{i=1}^{I_f-1} \frac{1}{I_f} \int_f \mathbf{u}|_{e_1} \cdot \mathbf{n}_{\partial e_1}\, dl - \sum_{i=1}^{I_f-1} \frac{1}{I_f} \int_f \mathbf{u}|_{e_{i+1}} \cdot \mathbf{n}_{\partial e_{i+1}}\, dl =$$
$$= \left((I_f - 1)\frac{1}{I_f} + \frac{1}{I_f}\right) \int_f \mathbf{u}|_{e_1} \cdot \mathbf{n}_{\partial e_1}\, dl = \int_f \mathbf{u}|_{e_1} \cdot \mathbf{n}_{\partial e_1}\, dl$$

for $j = 1$, using the normal trace continuity of $\mathbf{u}$ expressed by $\sum_{i=1}^{I_f} \int_f \mathbf{u}|_{e_i} \cdot \mathbf{n}_{\partial e_i}\, dl = 0$. Similarly, we have

$$(I_f - 2)\frac{1}{I_f} \int_f \mathbf{u}|_{e_1} \cdot \mathbf{n}_{\partial e_1}\, dl + \frac{1}{I_f} \int_f \mathbf{u}|_{e_1} \cdot \mathbf{n}_{\partial e_1}\, dl + \frac{1}{I_f} \int_f \mathbf{u}|_{e_j} \cdot \mathbf{n}_{\partial e_j}\, dl -$$
$$-(I_f - 1)\frac{1}{I_f} \int_f \mathbf{u}|_{e_1} \cdot \mathbf{n}_{\partial e_1}\, dl + (I_f - 1)\frac{1}{I_f} \int_f \mathbf{u}|_{e_j} \cdot \mathbf{n}_{\partial e_j}\, dl = \int_f \mathbf{u}|_{e_j} \cdot \mathbf{n}_{\partial e_j}\, dl$$

for $j \geq 2$, and thus the proof is completed.

Lemma 9. *Even for the considered special function spaces and their finite dimensional subspaces, we have*

$$\begin{array}{ccc} \mathbf{H}(grad, \mathcal{S}) & \xrightarrow{\text{div}} & L^2(\mathcal{S}) \\ \downarrow \pi_h & & \downarrow P_h \\ \mathbf{RT}_0^0(\mathcal{T}_h) & \xrightarrow{\text{div}} & M_{-1}^0(\mathcal{T}_h) \end{array}, \tag{20}$$

i.e. the commutativity diagram property, where π_h is the global interpolation operator defined by (19), and P_h is the $L^2(\mathcal{S})$-orthogonal projection onto $M_{-1}^0(\mathcal{T}_h)$.

Proof. The proof is easy using the previous lemma and the validity of the commutativity diagram property for the local interpolation operator, see e.g. [9, Section 3.4.2].

Definition 10. As the lowest order Raviart–Thomas mixed approximation of the the problem (14), (15), we understand functions $\mathbf{u}_{0,h} \in \mathbf{RT}_{0,N}^0(\mathcal{T}_h)$ and $p_h \in M_{-1}^0(\mathcal{T}_h)$ satisfying

$$(\mathbf{A}\mathbf{u}_{0,h}, \mathbf{v}_h)_{0,\mathcal{S}} - (\nabla \cdot \mathbf{v}_h, p_h)_{0,\mathcal{S}} = -\langle \mathbf{v}_h \cdot \mathbf{n}, p_D \rangle_{\Lambda_D} + (\nabla \cdot \mathbf{v}_h, z)_{0,\mathcal{S}} - \tag{21}$$
$$-\langle \mathbf{v}_h \cdot \mathbf{n}, z \rangle_{\partial\mathcal{S}} - (\mathbf{A}\tilde{\mathbf{u}}, \mathbf{v}_h)_{0,\mathcal{S}} \qquad \forall\, \mathbf{v}_h \in \mathbf{RT}_{0,N}^0(\mathcal{T}_h)\,,$$

$$-(\nabla \cdot \mathbf{u}_{0,h}, \phi_h)_{0,\mathcal{S}} = -(q, \phi_h)_{0,\mathcal{S}} + (\nabla \cdot \tilde{\mathbf{u}}, \phi_h)_{0,\mathcal{S}} \qquad \forall \phi_h \in M_{-1}^0(\mathcal{T}_h)\,. \tag{22}$$

Theorem 11. *The problem (21), (22) has a unique solution.*

Proof. Let us denote $\mathbf{V}_h = \mathbf{RT}^0_{0,N}(\mathcal{T}_h)$, $\Phi_h = M^0_{-1}(\mathcal{T}_h)$ and $\mathbf{W}_h = \{\mathbf{v}_h \in \mathbf{V}_h \ ; \ b(\mathbf{v}_h, \phi_h) = 0 \ \forall \phi_h \in \Phi_h\}$. As $\mathbf{V}_h \subset \mathbf{V}$, $\Phi_h \subset \Phi$, the (bi)linearity and continuity of the forms $a(\cdot,\cdot)$, $b(\cdot,\cdot)$ and of the functionals $f(\cdot)$ and $g(\cdot)$ from Theorem 5 holds also on $\mathbf{V}_h$ and Φ_h. Since $\mathbf{W}_h \subset \mathbf{W}$, also the coercivity of the form $a(\cdot,\cdot)$ is assured. For the discrete inf–sup condition, essential is the commutativity diagram property expressed by (20), at least for the case $\Lambda_N = \emptyset$. For the case $\Lambda_N \neq \emptyset$, a special procedure has to be carried out, cf. [11], pages 587-588.

5.3 Error Estimates

If the solution $(\mathbf{u}_0, p) \in \mathbf{V} \times \Phi$ of (14), (15) is such that $(\mathbf{u}_0, p) \in \mathbf{H}(grad, \mathcal{S}) \times H^1(\mathcal{S})$ and $\nabla \cdot \mathbf{u}_0 \in H^1(\mathcal{S})$ and if $(\mathbf{u}_{0,h}, p_h) \in \mathbf{V}_h \times \Phi_h$ is the solution of (21), (22), then

$$\|\mathbf{u}_0 - \mathbf{u}_{0,h}\|_{\mathbf{H}(div,\mathcal{S})} + \|p - p_h\|_{0,\mathcal{S}} \leq Ch(|p|_{1,\mathcal{S}} + |\mathbf{u}_0|_{1,\mathcal{S}} + |\nabla \cdot \mathbf{u}_0|_{1,\mathcal{S}}) \,, \tag{23}$$

where the constant C does not depend on h and $|\varphi|_{1,\mathcal{S}} = \|\nabla\varphi\|_{0,\mathcal{S}}$, $|\mathbf{u}|^2_{1,\mathcal{S}} = \sum_{i=1}^2 |\mathbf{u}_i|^2_{1,\mathcal{S}}$ (see [11], Theorem 13.2).

5.4 Hybridization of the Mixed Method

If $f \in \Lambda_h$, we define first the space $M^0(f)$ of functions constant on this edge and finally, on the edges structure $\Lambda_{h,D}$ defined by (9),

$$\begin{aligned} M^0_{-1}(\Lambda_{h,D}) \equiv \{\mu_h : \Lambda_h \to \mathbb{R} \,;\ \mu_h|_f \in M^0(f) \quad \forall f \in \Lambda_h \,, \\ \mu_h|_f = 0 \quad \forall f \in \Lambda_D\} \,. \end{aligned} \tag{24}$$

It now follows immediately that if $\mathbf{v}_h \in \mathbf{RT}^0_{-1}(\mathcal{T}_h)$, then $\mathbf{v}_h \in \mathbf{RT}^0_{0,N}(\mathcal{T}_h)$ if and only if

$$\sum_{e \in \mathcal{T}_h} \langle \mathbf{v}_h \cdot \mathbf{n}, \lambda_h \rangle_{\partial e \cap \Lambda_{h,D}} = 0 \quad \forall \lambda_h \in M^0_{-1}(\Lambda_{h,D}) \,,$$

which allows us to state the hybrid version of the lowest order Raviart–Thomas mixed method:

Definition 12. As the lowest order Raviart–Thomas mixed-hybrid approximation of the the problem (14), (15), we understand functions $\mathbf{u}_{0,h} \in \mathbf{RT}^0_{-1}(\mathcal{T}_h)$, $p_h \in M^0_{-1}(\mathcal{T}_h)$, and $\lambda_h \in M^0_{-1}(\Lambda_{h,D})$ satisfying

$$\begin{aligned} \sum_{e \in \mathcal{T}_h} \{(\mathbf{A}\mathbf{u}_{0,h}, \mathbf{v}_h)_{0,e} - (\nabla \cdot \mathbf{v}_h, p_h)_{0,e} + \langle \mathbf{v}_h \cdot \mathbf{n}, \lambda_h \rangle_{\partial e \cap \Lambda_{h,D}}\} = \\ = \sum_{e \in \mathcal{T}_h} \{-\langle \mathbf{v}_h \cdot \mathbf{n}, p_D \rangle_{\partial e \cap \Lambda_D} + (\nabla \cdot \mathbf{v}_h, z)_{0,e} - \langle \mathbf{v}_h \cdot \mathbf{n}, z \rangle_{\partial e} - (\mathbf{A}\tilde{\mathbf{u}}, \mathbf{v}_h)_{0,e}\} \\ \forall \, \mathbf{v}_h \in \mathbf{RT}^0_{-1}(\mathcal{T}_h) \,, \end{aligned} \tag{25}$$

$$\begin{aligned} -\sum_{e \in \mathcal{T}_h} (\nabla \cdot \mathbf{u}_{0,h}, \phi_h)_{0,e} = -\sum_{e \in \mathcal{T}_h} \{(q, \phi_h)_{0,e} - (\nabla \cdot \tilde{\mathbf{u}}, \phi_h)_{0,e}\} \\ \forall \phi_h \in M^0_{-1}(\mathcal{T}_h) \,, \end{aligned} \tag{26}$$

$$\sum_{e\in\mathcal{T}_h}\langle \mathbf{u}_{0,h}\cdot\mathbf{n},\mu_h\rangle_{\partial e\cap\Lambda_{h,D}} = \sum_{e\in\mathcal{T}_h}\{\langle u_N,\mu_h\rangle_{\partial e\cap\Lambda_N} - \langle\tilde{\mathbf{u}}\cdot\mathbf{n},\mu_h\rangle_{\partial e\cap\Lambda_{h,D}}\}$$
$$\forall\mu_h\in M^0_{-1}(\Lambda_{h,D})\,. \tag{27}$$

Due to the previously mentioned, the triple $\mathbf{u}_{0,h}$, p_h, λ_h surely exist and is unique, $\mathbf{u}_{0,h}$ and p_h are moreover at the same time the unique solutions of (21), (22); moreover, the multiplier λ_h is an approximation of the trace of p on all edges from $\Lambda_{h,D}$. Consequently, all error estimates from Section 5.3 are valid also for the mixed-hybrid solution triple $\mathbf{u}_{0,h}, p_h, \lambda_h$ and we have the following theorem:

Theorem 13. *The problem* (25) – (27) *has a unique solution.*

6 Mixed-hybrid FEM

We will use in this part the mixed-hybrid finite element method as introduced by [8] to treat our problem of steady saturated fracture flow. In fact, its use is more straightforward in the given case, since it handles even the case of one edge belonging to three or more triangles without any changes of formulation – through additional summation equation assuring the mass balance condition on inner edges.

6.1 Weak Mixed-hybrid Solution

We define the space

$$\mathbf{W}_D(\mathcal{T}_h) = \mathbf{H}(div,\mathcal{T}_h)\times L^2(\mathcal{S})\times H^{\frac{1}{2}}(\Lambda_{h,D}) \tag{28}$$

with the norm $\|\mathbf{w}\|^2_{\mathbf{W}_D(\mathcal{T}_h)} = \|\mathbf{v}\|^2_{\mathbf{H}(div,\mathcal{T}_h)} + \|\phi\|^2_{0,\mathcal{S}} + |\mu|^2_{\frac{1}{2},\Lambda_{h,D}}$. On $\mathbf{W}_D(\mathcal{T}_h)\times\mathbf{W}_D(\mathcal{T}_h)$, we define a bilinear form $\mathcal{B}$,

$$\mathcal{B}(\widehat{\mathbf{w}},\mathbf{w}) = \sum_{e\in\mathcal{T}_h}\Big\{(\mathbf{A}\mathbf{u},\mathbf{v})_{0,e} - (\nabla\cdot\mathbf{v},p)_{0,e} + \langle\mathbf{v}\cdot\mathbf{n},\lambda\rangle_{\partial e\cap\Lambda_{h,D}} - \tag{29}$$
$$-(\nabla\cdot\mathbf{u},\phi)_{0,e} + \langle\mathbf{u}\cdot\mathbf{n},\mu\rangle_{\partial e\cap\Lambda_{h,D}} - \langle\sigma\lambda,\mu\rangle_{\partial e\cap\Lambda_N}\Big\}$$

and on $\mathbf{W}_D(\mathcal{T}_h)$ a linear functional $\mathcal{Q}$,

$$\mathcal{Q}(\mathbf{w}) = \sum_{e\in\mathcal{T}_h}\Big\{-\langle\mathbf{v}\cdot\mathbf{n},p_D\rangle_{\partial e\cap\Lambda_D} + (\nabla\cdot\mathbf{v},z)_{0,e} - \langle\mathbf{v}\cdot\mathbf{n},z\rangle_{\partial e} - \tag{30}$$
$$-(q,\phi)_{0,e} + \langle u_N-\sigma p_D,\mu\rangle_{\partial e\cap\Lambda_N}\Big\}\,,$$

where $\widehat{\mathbf{w}} = (\mathbf{u},p,\lambda)\in\mathbf{W}_D(\mathcal{T}_h)$ and $\mathbf{w} = (\mathbf{v},\phi,\mu)\in\mathbf{W}_D(\mathcal{T}_h)$.

Definition 14. As a weak mixed-hybrid solution of the steady saturated fracture flow problem described by (2) – (4), we understand a function $\widehat{\mathbf{w}} = (\mathbf{u},p,\lambda)\in\mathbf{W}_D(\mathcal{T}_h)$ satisfying

$$\mathcal{B}(\widehat{\mathbf{w}},\mathbf{w}) = \mathcal{Q}(\mathbf{w})\qquad\forall\,\mathbf{w} = (\mathbf{v},\phi,\mu)\in\mathbf{W}_D(\mathcal{T}_h)\,. \tag{31}$$

Our general requirements are $A_{ij}(\mathbf{x}) \in L^\infty(\mathcal{S})$, $q \in L_2(\mathcal{S})$, $p_D \in H^{\frac{1}{2}}(\Lambda_D \cup \Lambda_N)$, $u_N \in H^{-\frac{1}{2}}(\Lambda_N)$ and $\sigma \in L^\infty(\Lambda_N)$, $0 \leq \sigma \leq \sigma_M$.

Theorem 15. *The problem (31) has a unique solution.*

Proof. The problem (31) is the same as originally studied by Oden and Lee in [8], except of incorporation of Newton boundary condition and occurrence of the vertical coordinate z. Using the existence and uniqueness of the primal solution even in our geometrical situation, there are no complications to show that the form $\mathcal{B}(\cdot,\cdot)$ is a bilinear continuous form on $\mathbf{W}_D(\mathcal{T}_h) \times \mathbf{W}_D(\mathcal{T}_h)$, satisfying the inf–sup condition of the type (16), and that the functional $\mathcal{Q}(\cdot)$ is a linear continuous functional on $\mathbf{W}_D(\mathcal{T}_h)$. The existence and uniqueness follows by the theory of Babuška, see [1, Theorem 2.1].

6.2 Mixed-hybrid Finite Element Approximation

We equip the space $M^0_{-1}(\Lambda_{h,D})$ of edge-wise constant functions defined by (24) with the norm

$$|\mu_h|^2_{*\frac{1}{2},\Lambda_{h,D}} = \sum_{e\in\mathcal{T}_h} |\mu_h|^2_{*\frac{1}{2},\partial e}\,, \tag{32}$$

where $|\mu_h|_{*\frac{1}{2},\partial e} = |\mu_h^*|_{\frac{1}{2},\partial e}$ with $\mu_h^* \in H^{\frac{1}{2}}(\partial e)$, μ_h^* edge-wise linear and satisfying $\int_{\partial e_i} \mu_h \, dl = \int_{\partial e_i} \mu_h^* \, dl$, $i \in \{1,2,3\}$, where ∂e_i are the sides of the triangle e. One can show that such definition is correct. We can now define the finite-dimensional approximation space

$$\mathbf{W}^h_D(\mathcal{T}_h) = \mathbf{RT}^0_{-1}(\mathcal{T}_h) \times M^0_{-1}(\mathcal{T}_h) \times M^0_{-1}(\Lambda_{h,D})$$

equipped with the norm $\|\mathbf{w}_h\|^2_{\mathbf{W}^h_D(\mathcal{T}_h)} = \|\mathbf{v}_h\|^2_{\mathbf{H}(div,\mathcal{T}_h)} + \|\phi_h\|^2_{0,\mathcal{S}} + |\mu_h|^2_{*\frac{1}{2},\Lambda_{h,D}}$, $\mathbf{w}_h = (\mathbf{v}_h, \phi_h, \mu_h) \in \mathbf{W}^h_D(\mathcal{T}_h)$.

Definition 16. As the lowest order Raviart–Thomas mixed-hybrid approximation of the the problem (31), we understand a function $\widehat{\mathbf{w}}_h = (\mathbf{u}_h, p_h, \lambda_h) \in \mathbf{W}^h_D(\mathcal{T}_h)$ satisfying

$$\mathcal{B}(\widehat{\mathbf{w}}_h, \mathbf{w}_h) = \mathcal{Q}(\mathbf{w}_h) \qquad \forall\, \mathbf{w}_h = (\mathbf{v}_h, \phi_h, \mu_h) \in \mathbf{W}^h_D(\mathcal{T}_h)\,. \tag{33}$$

Theorem 17. *The problem (33) has a unique solution.*

Proof. Using the definition of the norm (32), it is rather elaborate to show that the form $\mathcal{B}(\cdot,\cdot)$ is a bilinear continuous form also on $\mathbf{W}^h_D(\mathcal{T}_h) \times \mathbf{W}^h_D(\mathcal{T}_h)$, satisfying the discrete inf–sup condition, and that the functional $\mathcal{Q}(\cdot)$ is a linear continuous functional also on $\mathbf{W}^h_D(\mathcal{T}_h)$. Special qualities of the space $\mathbf{RT}^0(e)$ are used while replacing edge-wise constant μ_h by its edge-wise linear counterpart $\mu_h^* \in H^{\frac{1}{2}}(\partial e)$ in the proofs.

Remark 18. The definition of the norm (32) for $\mu_h \in M^0_{-1}(\Lambda_{h,D})$ is necessary. The form $\mathcal{B}(\cdot,\cdot)$ is not a continuous form on $\mathbf{W}^h_D(\mathcal{T}_h) \times \mathbf{W}^h_D(\mathcal{T}_h)$ equipped with the norm $\|\mu_h\|^2_{0,\Lambda_{h,D}} = \sum_{f\in\Lambda_{h,D}} \|\mu_h\|^2_{0,f}$ for μ_h. If we improve the norm on $\mathbf{W}^h_D(\mathcal{T}_h)$ as $\|\mathbf{w}_h\|^2_{\mathbf{W}^h_D(\mathcal{T}_h)} = \|\mathbf{v}_h\|^2_{\mathbf{H}(div,\mathcal{T}_h)} + \|\mathbf{v}_h\cdot\mathbf{n}\|^2_{0,\Lambda_h} + \|\phi_h\|^2_{0,\mathcal{S}} + \|\mu_h\|^2_{0,\Lambda_{h,D}}$, the form $\mathcal{B}(\cdot,\cdot)$ gets continuous, but the discrete inf–sup condition is not satisfied with a constant independent of h, all owing to the mixture of the spaces $\mathbf{RT}^0(e)$ approximating $\mathbf{H}(div,e)$ with generally only $\mathbf{u}\cdot\mathbf{n} \in H^{-\frac{1}{2}}(\partial e)$, $\mathbf{u}\in\mathbf{H}(div,e)$, and $M^0_{-1}(\partial e)$ of edge-wise constant functions belonging generally only to $L^2(\partial e)$. By the definition (32), we "skip" into necessary $H^{\frac{1}{2}}(\partial e)$.

6.3 Error Estimates

We shall notice first that we are dealing with a *nonconform* approximation. We have approximated the space $H^{\frac{1}{2}}(\Lambda_{h,D})$ given by (10) by the space $M^0_{-1}(\Lambda_{h,D})$ given by (24). We set

$$\mathcal{X} = \left\{\mathbf{v}\in\mathbf{H}(div,\mathcal{T}_h)\,;\,\mathbf{v}\cdot\mathbf{n}\in L^2(\Lambda_{h,D})\right\}\times\left\{\phi\in L^2(\mathcal{S})\right\}\times$$
$$\times\left\{\mu+\mu_h\,;\,\mu\in H^{\frac{1}{2}}(\Lambda_{h,D})\,,\ \mu_h\in M^0_{-1}(\Lambda_{h,D})\right\},$$

$\|\mathbf{w}\|^2_{\mathcal{X}} = \|\mathbf{v}\|^2_{\mathbf{H}(div,\mathcal{T}_h)} + \|\phi\|^2_{0,\mathcal{S}} + |\mu+\mu_h|^2_{*\frac{1}{2},\Lambda_{h,D}}$, and after some tedious manipulations, we come to the bilinearity and continuity (with the constant $C_1^{\mathcal{X}}$) of the form $\mathcal{B}(\cdot,\cdot)$ on $\mathcal{X}\times\mathbf{W}^h_D(\mathcal{T}_h)$. The error estimate is consequently of the form

$$\|\widehat{\mathbf{w}}-\widehat{\mathbf{w}}_h\|_{\mathcal{X}} \le$$
$$\le\left(1+\frac{C_1^{\mathcal{X}}}{C_2^d}\right)\inf_{\mathbf{w}_h\in\mathbf{W}^h_D(\mathcal{T}_h)}\|\widehat{\mathbf{w}}-\mathbf{w}_h\|_{\mathcal{X}} + \frac{1}{C_2^d}\sup_{\mathbf{w}_h\in\mathbf{W}^h_D(\mathcal{T}_h)}\frac{|\mathcal{Q}(\mathbf{w}_h)-\mathcal{B}(\widehat{\mathbf{w}},\mathbf{w}_h)|}{\|\mathbf{w}_h\|_{\mathcal{X}}}\,,$$

$\widehat{\mathbf{w}} = (\mathbf{u},p,\lambda)\in\mathbf{W}_D(\mathcal{T}_h)\bigcap\mathcal{X}$ being the unique weak mixed-hybrid solution defined by (31), $\widehat{\mathbf{w}}_h = (\mathbf{u}_h,p_h,\lambda_h)\in\mathbf{W}^h_D(\mathcal{T}_h)$ the mixed-hybrid approximation defined by (33), and C_2^d being the constant from the discrete inf–sup condition. However, due to the restriction $\mathbf{v}\cdot\mathbf{n}\in L^2(\Lambda_{h,D})$ (necessary to give the sense to the term $\mathcal{B}(\widehat{\mathbf{w}},\mathbf{w}_h)$ from the nonconform error estimate), we come to

$$\sup_{\mathbf{w}_h\in\mathbf{W}^h_D(\mathcal{T}_h)}\frac{|\mathcal{Q}(\mathbf{w}_h)-\mathcal{B}(\widehat{\mathbf{w}},\mathbf{w}_h)|}{\|\mathbf{w}_h\|_{\mathcal{X}}} = \sup_{\mu_h\in M^0_{-1}(\Lambda_{h,D})}\frac{|\sum_{e\in\mathcal{T}_h}\{\langle\mathbf{u}\cdot\mathbf{n},\mu_h\rangle_{\partial e\setminus\partial\mathcal{S}}+}{}$$
$$\frac{+\langle\mathbf{u}\cdot\mathbf{n}-u_N,\mu_h\rangle_{\partial e\cap\Lambda_N}+\langle\sigma(p_D-\lambda),\mu_h\rangle_{\partial e\cap\Lambda_N}\}|}{|\mu_h|_{*\frac{1}{2},\Lambda_{h,D}}} = 0$$

and thus the final error estimate has the form

$$\|\widehat{\mathbf{w}}-\widehat{\mathbf{w}}_h\|_{\mathcal{X}} \le \left(1+\frac{C_1^{\mathcal{X}}}{C_2^d}\right)Ch\sqrt{(|\mathbf{u}|_{1,\mathcal{S}}+|\nabla\cdot\mathbf{u}|_{1,\mathcal{S}})^2+\|p\|^2_{2,\mathcal{S}}}\,, \tag{34}$$

for $\mathbf{u}\in\mathbf{H}(grad,\mathcal{S})$, $\nabla\cdot\mathbf{u}\in H^1(\mathcal{S})$ and $p\in H^2(\mathcal{S})$ except of the previous requirements, the constant C independent of h. This means that we have the $O(h)$ accuracy, however not for the edge-wise constant μ_h, but for its extension μ_h^*.

7 Model Problems

We consider two simple model problems in this section. The first model problem is a model problem on a system $\mathcal{S}$, where at most two polygons intersect through one edge, i.e. almost classical planar case; we call this as *special geometrical situation*. In the second model problem, one edge is common to four polygons; we call this situation, the kernel of what has been investigated in this contribution, as a *general geometrical situation*. All the computations were done in double precision on a personal computer, the resulting symmetric indefinite systems of linear equations were solved by the solver GI8 of the Institute of Computer Science, Academy of Sciences of the Czech Republic, see [6]. This is based on the sequential elimination onto a system with Schur's complement and subsequent solution of this system by a specially preconditioned conjugate gradients method. The solver accuracy was set to 10^{-8}.

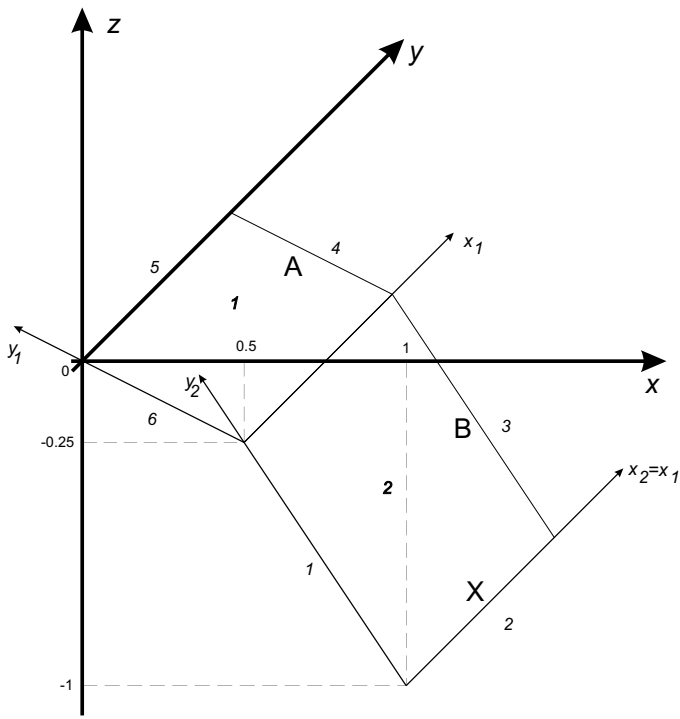

Fig. 1. Model Problem I – Special Geometrical Situation

7.1 Model Problem I – Special Geometrical Situation

The problem with the system $\mathcal{S}$ viewed in Figure 1 is as follows:

$$\mathcal{S} = \overline{\alpha_1} \bigcup \overline{\alpha_2} \setminus \partial\mathcal{S}\,,$$

$$\begin{aligned} \mathbf{u} &= -\Big(\nabla p + \nabla z\Big) \quad \text{in} \quad \mathcal{S}\,, \\ \nabla \cdot \mathbf{u} &= 0 \quad \text{in} \quad \mathcal{S}\,, \end{aligned}$$

$$\begin{aligned} p = 0 \quad \text{in} \quad \Lambda_1 \quad , \quad p = 0 \quad \text{in} \quad \Lambda_2 \\ \mathbf{u}\cdot\mathbf{n} = 0 \quad \text{in} \quad \Lambda_3 \quad , \quad \mathbf{u}\cdot\mathbf{n} = 0 \quad \text{in} \quad \Lambda_4 \\ p = \sin\Big(\tfrac{\pi x_1}{2X}\Big)\sinh\Big(\tfrac{\pi(A+B)}{2X}\Big) + S\cdot A \quad \text{in} \quad \Lambda_5 \quad , \quad p = S\cdot y_1 \quad \text{in} \quad \Lambda_6\,. \end{aligned}$$

The exact solutions in α_1 can be easily found as

$$\begin{aligned} p_{\alpha_1} &= \sin\Big(\frac{\pi x_1}{2X}\Big)\sinh\Big(\frac{\pi(y_1+B)}{2X}\Big) + S\cdot y_1\,, \\ \mathbf{u}_{\alpha_1} &= \Big(-\frac{\pi}{2X}\cos\Big(\frac{\pi x_1}{2X}\Big)\sinh\Big(\frac{\pi(y_1+B)}{2X}\Big), \\ &\quad -\frac{\pi}{2X}\sin\Big(\frac{\pi x_1}{2X}\Big)\cosh\Big(\frac{\pi(y_1+B)}{2X}\Big) - S - \nabla z^y_{\alpha_1}\Big)\,, \end{aligned}$$

where $\nabla z_{\alpha_1} = (0, \nabla z^y_{\alpha_1})$, $S + \nabla z^y_{\alpha_1} = \nabla z^y_{\alpha_2}$, and we can see them in Figures 2 and 3. Notice the occurrence of the term S assuring the continuity of the velocity field because of different z gradients in α_1 and α_2.

The following table gives pressure, velocity, and pressure trace errors in the fracture α_1. There is the $O(h)$ convergence in pressure, velocity, and pressure trace in $|\cdot|_{*\frac{1}{2},\Lambda_{h,D}}$ norm, but only $O(h^{\frac{1}{2}})$ in pressure trace in $\|\cdot\|_{0,\Lambda_{h,D}}$ norm.

N	triangles	$\|p-p_h\|_{0,\mathcal{S}}$	$\|\mathbf{u}-\mathbf{u}_h\|_{\mathbf{H}(div,\mathcal{T}_h)}$	$\|\lambda-\lambda_h\|_{0,\Lambda_{h,D}}$	$\|\lambda-\lambda_h\|_{*\frac{1}{2},\Lambda_{h,D}}$
2	8×2	0.4481	1.2236	1.4984	1.2236
4	32×2	0.2212	0.6262	1.0564	0.6262
8	128×2	0.1102	0.3150	0.7509	0.3150
16	512×2	0.0550	0.1577	0.5332	0.1577
32	2048×2	0.0275	0.0789	0.3779	0.0789
64	8192×2	0.0138	0.0394	0.2676	0.0394
128	32768×2	0.0069	0.0197	0.1893	0.0197
256	131072×2	0.0034	0.0099	0.1339	0.0099

Table 1. Pressure, Velocity, and Pressure Trace Errors in α_1 for the Special Geometrical Situation, Model Problem I

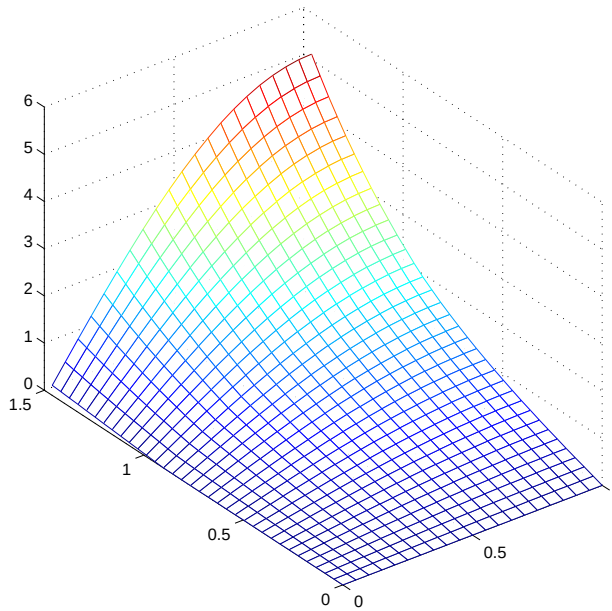

Fig. 2. Exact Pressure Graph in Fractures α_1 and α_2, Model Problems I and II

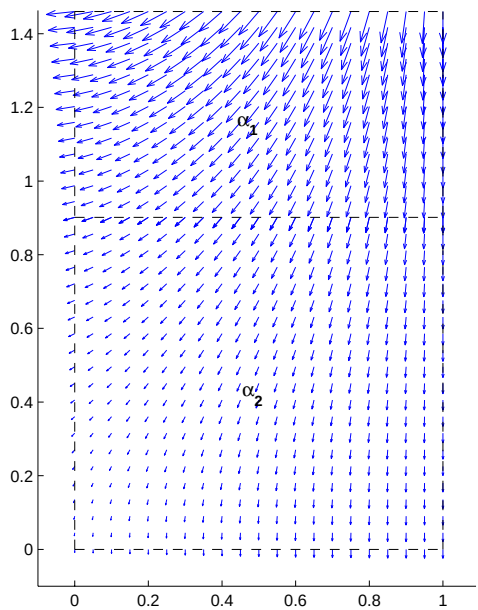

Fig. 3. Exact Velocity Graph in Fractures α_1 and α_2, Model Problems I and II.

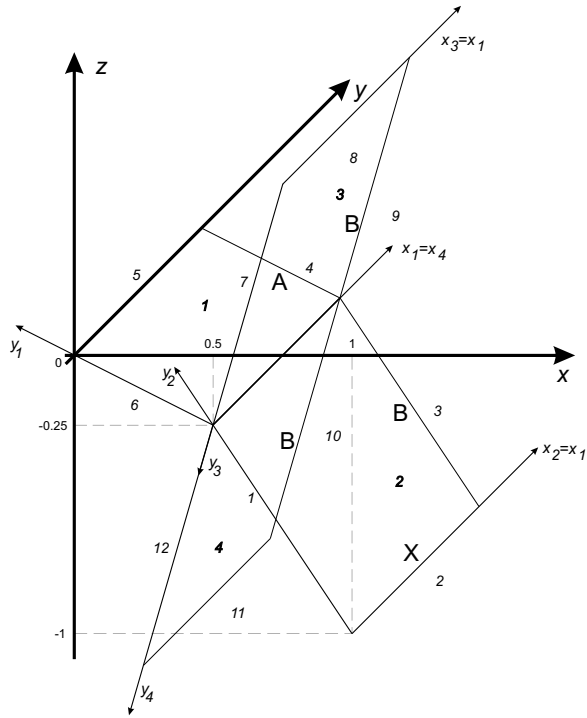

Fig. 4. Model Problem II – General Geometrical Situation

7.2 Model Problem II – General Geometrical Situation

The system $\mathcal{S}$ for this model problem is viewed in Figure 4. We have

$$\mathcal{S} = \overline{\alpha_1} \bigcup \overline{\alpha_2} \bigcup \overline{\alpha_3} \bigcup \overline{\alpha_4} \setminus \partial\mathcal{S}\,,$$

$$\begin{aligned} \mathbf{u} &= -\Big(\nabla p + \nabla z\Big) \quad \text{in} \quad \mathcal{S}\,, \\ \nabla \cdot \mathbf{u} &= 0 \quad \text{in} \quad \mathcal{S}\,, \end{aligned}$$

$$\begin{gathered} p = 0 \quad \text{in} \quad \Lambda_7 \quad , \quad p = 0 \quad \text{in} \quad \Lambda_8 \\ \mathbf{u} \cdot \mathbf{n} = 0 \quad \text{in} \quad \Lambda_9 \quad , \quad \mathbf{u} \cdot \mathbf{n} = 0 \quad \text{in} \quad \Lambda_{10} \\ p = \sin\Big(\tfrac{\pi x_4}{2X}\Big) \sinh\Big(\tfrac{\pi(B+B)}{2X}\Big) \quad \text{in} \quad \Lambda_{11} \quad , \quad p = 0 \quad \text{in} \quad \Lambda_{12}\,, \end{gathered}$$

and boundary conditions on Λ_1 – Λ_6 as for the model problem I. The exact solutions in α_1 and α_2 stay the same.

We give approximation errors in the first fracture α_1. As the exact solutions coincide for the model problems I a II, we can compare tables 1 and 2, i.e. special (almost classical, planar) and general (the situation characteristic for the investigated problem of the fracture flow) geometrical situations. A slight difference appears only for rough triangulations and disappears for the increasing N. Thus, demonstrated for these two model problems, the existence of triangulation edges common to three and more triangles does not influence the error, resp. convergence order. This was verified also for the pressure, velocity and pressure trace error distributions, as we can see in Figures 5, 6 and 7.

N	triangles	$\|p - p_h\|_{0,\mathcal{S}}$	$\|\mathbf{u} - \mathbf{u}_h\|_{\mathbf{H}(div,\mathcal{T}_h)}$	$\|\lambda - \lambda_h\|_{0,\Lambda_{h,D}}$	$\|\lambda - \lambda_h\|_{*\frac{1}{2},\Lambda_{h,D}}$
2	8×4	0.4445	1.2247	1.4973	1.2247
4	32×4	0.2212	0.6263	1.0562	0.6263
8	128×4	0.1102	0.3150	0.7509	0.3150
16	512×4	0.0550	0.1577	0.5332	0.1577
32	2048×4	0.0275	0.0789	0.3779	0.0789
64	8192×4	0.0138	0.0394	0.2676	0.0394
128	32768×4	0.0069	0.0197	0.1893	0.0197
256	131072×4	0.0034	0.0099	0.1339	0.0099

Table 2. Pressure, Velocity, and Pressure Trace Errors in α_1 for the General Geometrical Situation, Model Problem II

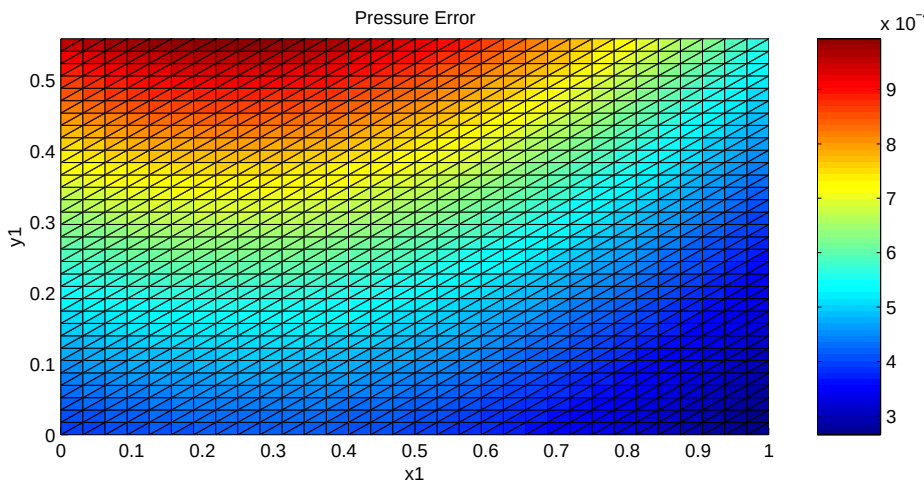

Fig. 5. Distribution of the Pressure Error in α_1, Model Problems I and II

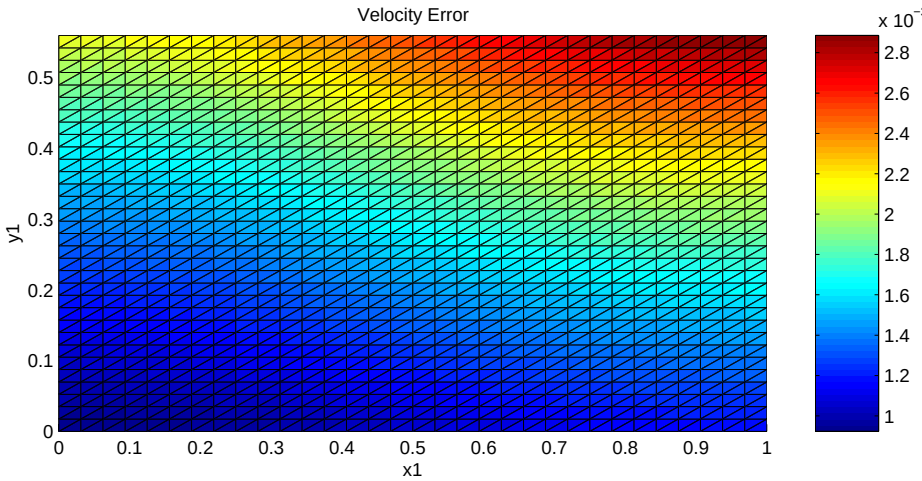

Fig. 6. Distribution of the Velocity Error in α_1, Model Problems I and II

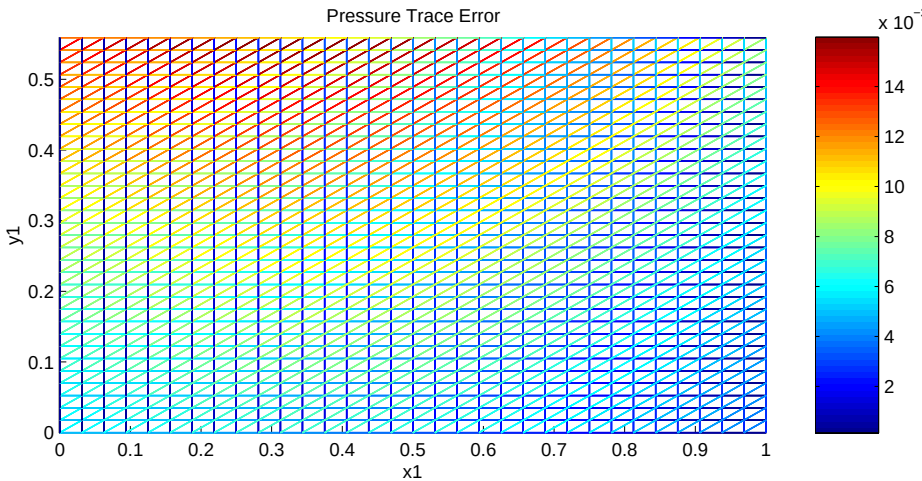

Fig. 7. Distribution of the "L^2" Pr. Trace Error in α_1, Model Problems I and II

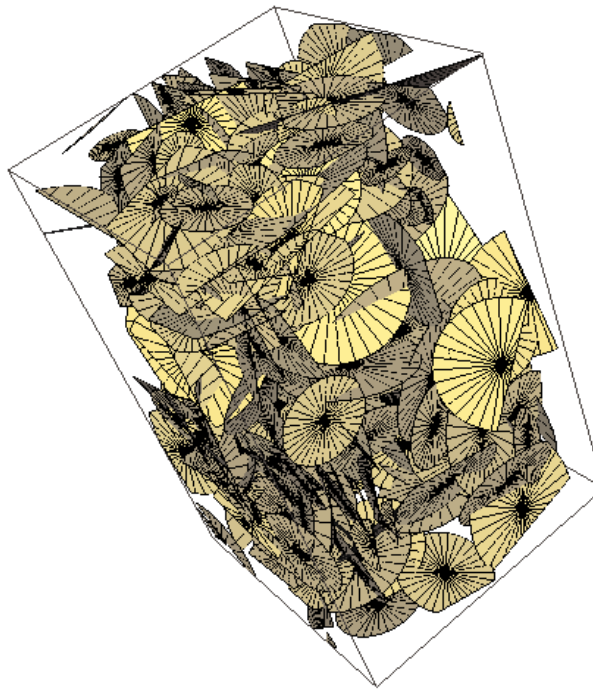

Fig. 8. Generated Fracture Network on a 5 × 5 × 8 m Domain

8 Simulation of a Real Situation: Stochastic Discrete Fracture Network Generation and Discretization

We describe in this section the preparation of the fracture network and its triangulation in real situations.

8.1 Stochastic Discrete Fracture Network Generation

In order to generate stochastic discrete fracture networks, an original software called **Fracture Network Generator** was developed. Each fracture (geological 3-D object) is in the generator approximated by a flat circle disk characterized by its *middle coordinates*, *radius*, *orientation*, possibly *hydraulic conductivity* or *aperture distribution* and *roughness*. Fractures are divided into four sets: *fractures in fracture zones*, *deterministically measured single fractures*, *hydraulically important fractures* and *other (common) fractures*. Fractures are further supposed to be divided into three types according to their mean orientation in 3-D cartesian coordinates [0,0,1], [0,1,0] or [1,0,0]. Each combination of set and type, except of

deterministically measured single fractures, is treated as an independent statistical population. Number of fractures and spacing determines *fracture frequency*, defined as amount of fractures per one depth meter in each part of the simulated domain. *Fracture lengths* are supposed as lognormally distributed, i.e. with the probability density function (p.d.f.) $f(x) = \frac{1}{\sigma\sqrt{2\pi}x} \exp(-(\ln x - \mu)^2/2\sigma^2)$. Concerning *orientations*, fractures are supposed to have the Fisher-von-Mises distribution $f(\alpha) = \frac{k}{\exp(k)} \exp(k \cos\alpha) \sin\alpha$ of angles α between fracture normal vectors and vectors of mean orientations.

In order to validate methods used for the statistical description and generating algorithms, χ^2 tests for each simulated variable were carried out, see [12]; we only have to put an emphasis on strictly distinguishing between real statistical characteristics and by "exploration boreholes" measured distributions, the latter of them being affected by a selective effect. Indeed, while drilling borehole, we have a bigger chance to intersect a larger fracture than a smaller one. We can see an example of a generated network in Figure 8.

8.2 Final Triangular Mesh Construction

Discretization of approximating circle disks into triangle elements has occurred as a crucial point. Although many algorithms solving the discretization of a given 2-D domain are known, only few of them are able to involve pre-defined interface lines, intersections of approximating circles in our case. The searched algorithm should be in addition capable to simplify the given geometrical situation (to save computer storage and avoid numerical faults and ill-conditioned resulting matrix), i.e. it can be only approximate; obtaining the initial mesh is also sufficient. In the **Fracture Network Generator**, an originally developed discretization algorithm is implemented. It contains of a *preliminary phase* and of an algorithm for triangulation of an arbitrary polygonally bounded domain with pre-defined interface lines (*triangulation algorithm*).

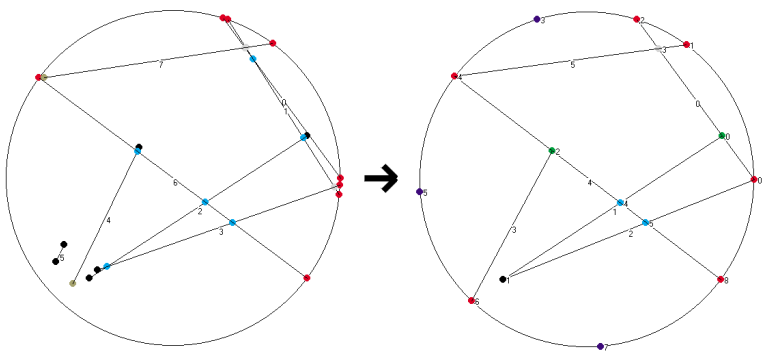

Fig. 9. 2-D Geometrical Simplifications

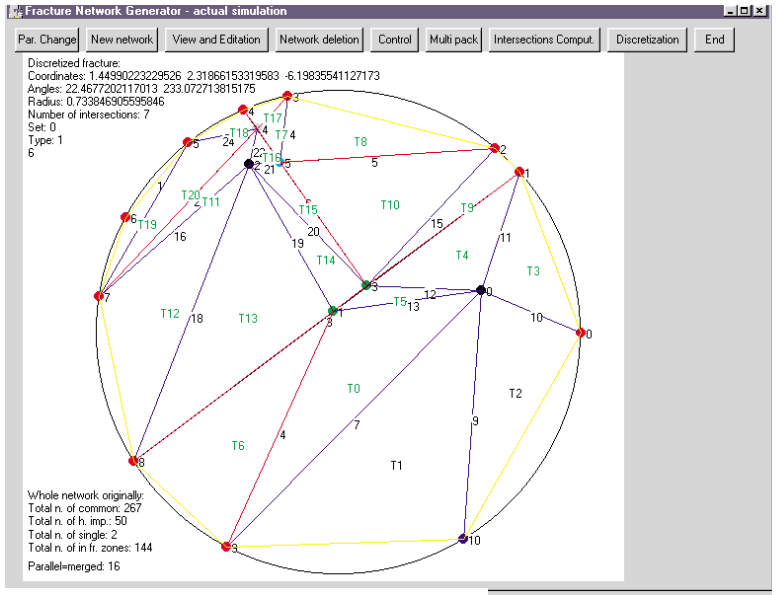

Fig. 10. Final Discretization of a Circle Disk

In the preliminary phase, identification and various geometrical simplifications are made. Close, almost parallel fractures are removed from the fracture population or equivalently replaced. 2-D geometrical simplifications (moving and stretching intersections in fracture planes) are carried out before the start of the actual triangulation algorithm; we can see an example of these simplifications in Figure 9. Using these 2-D geometrical simplifications has naturally non-trivial 3-D consequences - if the simplifications are used, then the real geometrical correspondence vanishes. It is then replaced by extra connectivity information.

The actual triangulation algorithm is based on combining the *Domain Decomposition Conception*, expressing that the domain is split into two parts along an intersection whenever possible, and adapted classical triangulation algorithm, *Advancing Front Method*. Many user's setting influencing incorporating the geometrical simplifications and thus the precision/complexity of the final triangulation are possible. An example of final triangulation of a random circle disk is in Fig. 10.

An on-element aperture distribution function is used after the discretization in order to assign to each triangle element an imaginary aperture. It is derived again from the Fisher-von-Mises distribution p.d.f., but depends also on the size of the given fracture and emplacement of the element inside the fracture. Based on the aperture and on a parameter describing roughness of the fracture walls, the element hydraulic conductivity can be later set, in order to simulate the "channeling effect" (the flow throughout a natural fracture is not evenly distributed throughout the whole fracture plane because of its non-constant aperture – channels of flow

occur). The fracture is, however, still supposed as planar. Data files with complete information about elements in the final triangular network (emplacement, aperture, roughness, hydraulic conductivity and connection to other elements) are the final results of the **Fracture Network Generator**. We can see the final triangular mesh of the network from Fig. 8 in Fig. 11. A colour gradiation is used in order to denote elements apertures.

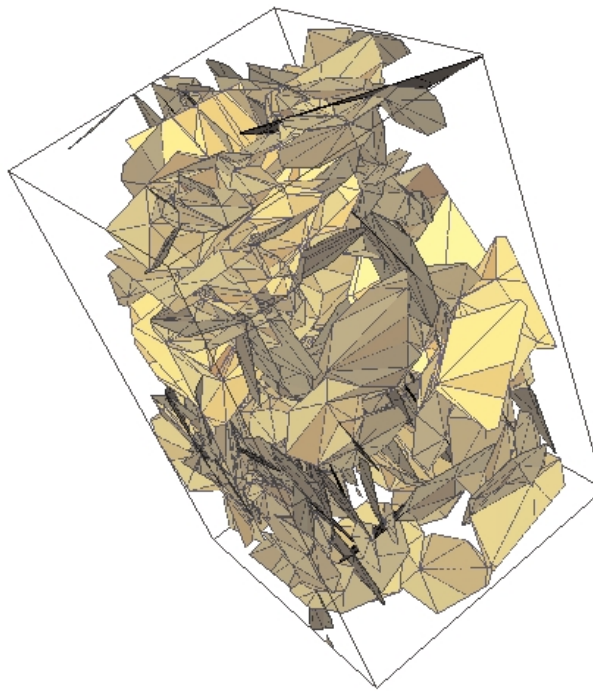

Fig. 11. Triangulation of the Network from Figure 8

9 Conclusion

In the submitted text, a discrete fracture network model of the fracture flow with existence and numerical analysis, examples of model problems, and description of application on real situations was introduced. The finite element method for numerical approximation was chosen so as to achieve the biggest possible accuracy. The mixed-hybrid approximation was chosen because it, unlike the primal approximation, assures mass balance on each element and its data structures are

though suitable for subsequent finite volume contaminant transport models, which are perspectively our main goal. In this approximation, the velocity is moreover computed directly and has good continuity rank, on the other hand, slightly bigger resulting matrix is the only drawback.

The mixed-hybrid weak formulation is much more straightforward in the given case, when three or more triangles can intersect through one edge in the discretization; it expresses directly the mass balance condition on such edges. However, the lowest order Raviart-Thomas mixed-hybrid approximation is a nonconform approximation to the weak mixed-hybrid solution, which causes difficulties while investigating its existence, uniqueness, and approximation error. Under the construction of special function spaces, mixed weak solution and approximation were established too, and their existence and uniqueness were shown using classical techniques.

Acknowledgement

This paper came to existence in framework of the project of the Grant Agency of the Czech Republic No. 205/00/0480. The last of the authors was also partially supported by the project No. J04/98:210000010 "Application of Mathematics in Technical Sciences" of the Government of the Czech Republic.

References

1. Babuška I., *Error-Bounds for Finite Element Method*, Numerische Mathematik **16** (1971), 322–333.
2. Cacas M. C., Ledoux E., De Marsily G., *Modelling Fracture Flow With a Stochastic Discrete Fracture Network: Calibration and Validation the Flow and the Transport Model*, Water Resources Research **26**, No 3, 1990, 479–489.
3. *Characterization and Evaluation of Sites for Deep Geological Disposal of Radioactive Waste in Fractured Rocks–Proceedings from The 3rd Äspö International Seminar*, Oskarshamn, June 10–12, SKB Technical Report 98-10, Stockholm, 1998.
4. Kaasschieter E. F., Huijben A. J. M., *Mixed-hybrid Finite Elements and Streamline Computation for the Potential Flow Problem*, Report PN 90-02-A, TNO Institute of Applied Geoscience, Delft, 1990.
5. Maryška J., Rozložník M., Tůma M., *Mixed-hybrid Finite Element Approximation of the Potential Fluid Flow Problem*, Journal of Computational and Applied Mathematics **63** (1995), 383–392.
6. Maryška J., Rozložník M., Tůma M., *Schur Complement Reduction in the Mixed-hybrid Finite Element Approximation of Darcy's Law: Rounding Error Analysis*, Technical Report TR-98-06, Swiss Center for Scientific Computing, Swiss Federal Institute of Technology, Zurich, 1998, 1–15.
7. Maryška J., Severýn O., Vohralík M., *Mixed-hybrid Model of the Fracture Flow*, Proceedings of international conference ALGORITMY 2000, Slovak Technical University, Bratislava, 2000, 75–84.

8. Oden J. T., Lee J. K., *Dual-mixed Hybrid Finite Element Method for Second-order Elliptic Problems*, in: Mathematical Aspects of Finite Element Methods (I. Galligani and E. Magenes, eds.), Lecture Notes in Math. Vol 606, Springer Verlag, Berlin, 1977, 275–291.
9. Quarteroni A., Valli A., *Numerical Approximation of Partial Differential Equations*, Springer-Verlag Berlin Heidelberg, Berlin, 1994.
10. Raviart P. A., Thomas J. M., *A Mixed Finite Element Method for Second-order Elliptic Problems*, in: Mathematical Aspects of Finite Element Methods (I. Galligani and E. Magenes, eds.), Lecture Notes in Math. Vol 606, Springer Verlag, Berlin, 1977, 292–315.
11. Roberts J. E., Thomas J. M., *Mixed and Hybrid Methods* in: Handbook of Numerical Analysis, vol. II, Finite Element Methods, Part 1 (P. G. Ciarlet and J. L. Lions, eds.), Elsevier Science Publishers B.V. (North-Holland), Amsterdam, 1991, 523–639.
12. Vohralík M., *Mixed-hybrid Model of the Fracture Flow*, Diploma Thesis, Faculty of Nuclear Sciences and Physical Engineering, Czech Technical University in Prague, Prague, 2000.
13. Vohralík M., *Modelling the Fracture Flow*, Proceedings of international conference SIMONA 2000, Technical University of Liberec, Liberec, 2000, 58–68.
14. Vohralík M., *Existence- and Error Analysis of the Mixed-hybrid Model of the Fracture Flow*, Technical Report MATH-NM-06-2001, Dresden University of Technology, Dresden, 2001.

S